Parameter optimization for through-focus scanning optical microscopy

Ravi Kiran Attota,[1,*] and Hyeonggon Kang[2]

[1]Engineering Physics Division, Physical Measurement Laboratory, National Institute of Standards and Technology, Gaithersburg, MD 20899, USA
[2]Currently with the Center for Nanotechnology, Department of Natural Sciences, Coppin State University Science and Technology Center, 2500 W. North Avenue, Baltimore, MD 21216, USA
[*]Ravikiran.Attota@nist.gov

Abstract: It is important to economically and non-destructively analyze three-dimensional (3-D) shapes of nanometer to micrometer scale objects with sub-nanometer measurement resolution for emerging high-volume nanomanufacturing, especially for process control. High-throughput through-focus scanning optical microscopy (TSOM) demonstrates promise for such applications. TSOM uses a conventional optical microscope for 3-D shape metrology by making use of the complete set of through-focus, four-dimensional optical data. However, a systematic study showing the effect of various parameters on the TSOM method is lacking. Here we present the optimization of the basic parameters such as illumination numerical aperture (NA), collection NA, focus step height, digital camera pixel size, illumination polarization, and illumination wavelength to achieve peak performance of the TSOM method.

OCIS codes: (120.0120) Instrumentation, measurement, and metrology; (120.3930) Metrological instrumentation; (180.5810) Scanning microscopy; (180.6900) Three-dimensional microscopy.

References and links

1. X. X. Zhang, H. Zhou, Z. H. Ge, A. Vaid, D. Konduparthi, C. Osorio, S. Ventola, R. Meir, O. Shoval, R. Kris, O. Adan, and M. Bar-Zvi, "Addressing FinFET metrology challenges in 1x node using tilt-beam critical dimension scanning electron microscope," J. Micro-Nanolith Mem. **13**(4), 041407 (2014).
2. X. X. Zhang, P. Snow, A. Vaid, E. Solecky, H. Zhou, Z. H. Ge, S. Yasharzade, O. Shoval, O. Adan, I. Schwarzband, and M. Bar-Zvi, "Solving next generation (1X node) metrology challenges using advanced CDSEM capabilities: tilt, high energy and backscatter imaging," Proc. SPIE **9424**, 94240G (2015).
3. H. Schroettner, M. Schmied, and S. Scherer, "Comparison of 3D surface reconstruction data from certified depth standards obtained by SEM and an infinite focus measurement machine (IFM)," Mikrochim. Acta **155**(1-2), 279–284 (2006).
4. C. Wang, R. L. Jones, E. K. Lin, W.-L. Wu, and J. Leu, "Small angle x-ray scattering measurements of lithographic patterns with sidewall roughness from vertical standing waves," Appl. Phys. Lett. **90**(19), 193122 (2007).
5. T. M. Bao, L. Mininni, and D. Dawson, "Improving sidewall profile metrology with enhanced 3D-AFM," Lithography Asia **2008**, 7140 (2008).
6. A. Punge, S. O. Rizzoli, R. Jahn, J. D. Wildanger, L. Meyer, A. Schönle, L. Kastrup, and S. W. Hell, "3D reconstruction of high-resolution STED microscope images," Microsc. Res. Tech. **71**(9), 644–650 (2008).
7. D. Wildanger, R. Medda, L. Kastrup, and S. W. Hell, "A compact STED microscope providing 3D nanoscale resolution," J. Microsc. **236**(1), 35–43 (2009).
8. V. M. J. I. Cuijpers, X. F. Walboomers, and J. A. Jansen, "Scanning electron microscopy stereoimaging for three-dimensional visualization and analysis of cells in tissue-engineered constructs: technical note," Tissue Eng. Part C Methods **17**(6), 663–668 (2011).
9. W. Häßler-Grohne, D. Huser, K. P. Johnsen, C. G. Frase, and H. Bosse, "Current limitations of SEM and AFM metrology for the characterization of 3D nanostructures," Meas. Sci. Technol. **22**(9), 094003 (2011).
10. J. A. Kramar, R. Dixson, and N. G. Orji, "Scanning probe microscope dimensional metrology at NIST," Meas. Sci. Technol. **22**(2), 024001 (2011).
11. N. G. Orji, R. G. Dixson, A. E. Vladar, and M. T. Postek, "Strategies for nanoscale contour metrology using critical dimension atomic force microscopy," Proc. SPIE **8105**, 810505 (2011).
12. J. Carrero and G. Percin, "Accurate optical CD profiler based on specialized finite element method," Proc. SPIE **8324**, 83240P (2012).
13. G. L. Dai, W. Hassler-Grohne, D. Huser, H. Wolff, J. Fluegge, and H. Bosse, "New developments at Physikalisch Technische Bundesanstalt in three-dimensional atomic force microscopy with tapping and torsion

#262754 Received 8 Apr 2016; revised 30 May 2016; accepted 30 May 2016; published 23 Jun 2016
(C) 2016 OSA

atomic force microscopy mode and vector approach probing strategy," J. Micro-Nanolith Mem. **11**(1), 011004 (2012).

14. J. L. Di, J. L. Zhao, and A. Asundi, "Compact digital holoscope with dual wavelength," Information Optics and Optical Data Storage Ii **8559**, 855908 (2012).
15. Y. Huang, Q. H. Han, Y. Q. Sui, C. J. Xu, X. Y. Meng, C. W. Li, and S. Ni, "OCD Metrology Evaluation of p-MOS silicon recess with three dimensional design pattern," ECS Trans. **44**, 1111–1116 (2012).
16. B. G. Kopek, G. Shtengel, C. S. Xu, D. A. Clayton, and H. F. Hess, "Correlative 3D superresolution fluorescence and electron microscopy reveal the relationship of mitochondrial nucleoids to membranes," Proc. Natl. Acad. Sci. U.S.A. **109**(16), 6136–6141 (2012).
17. N. G. Orji, R. G. Dixson, A. E. Vladar, B. Ming, and M. T. Postek, "Contour metrology using critical dimension atomic force microscopy," Proc. SPIE **8324**, 83240U (2012).
18. A. E. Vladar, P. Cizmar, J. S. Villarrubia, and M. T. Postek, "Can we get 3D CD metrology right?" Proc. SPIE **8324**, 832402 (2012).
19. H. Chouaib and Q. Zhao, "Nanoscale optical critical dimension measurement of a contact hole using deep ultraviolet spectroscopic ellipsometry," J. Vac. Sci. Technol. B **31**(1), 011803 (2013).
20. J. Li, O. Kritsun, P. Dasari, C. Volkman, T. Wallow, and J. T. Hu, "Evaluating scatterometry 3D capabilities for EUV," Proc. SPIE **8681**, 86810S (2013).
21. J. Qin, R. M. Silver, B. M. Barnes, H. Zhou, and F. Goasmat, "Fourier domain optical tool normalization for quantitative parametric image reconstruction," Appl. Opt. **52**(26), 6512–6522 (2013).
22. D. F. Sunday, M. R. Hammond, C. Q. Wang, W. L. Wu, R. J. Kline, and G. E. Stein, "Three-dimensional x-ray metrology for block copolymer lithography line-space patterns," J. Micro-Nanolith Mem. **12**(3), 031103 (2013).
23. A. Yamaguchi, T. Ohashi, T. Kawasaki, O. Inoue, and H. Kawada, "Three-dimensional profile extraction from CD-SEM image and top/bottom CD measurement by line-edge roughness analysis," Proc. SPIE **8681**, 86812Z (2013).
24. R. Chao, K. K. Kohli, Y. L. Zhang, A. Madan, G. R. Muthinti, A. J. Hong, D. Conklin, J. Holt, and T. C. Bailey, "Multitechnique metrology methods for evaluating pitch walking in 14 nm and beyond FinFETs," J. Micro-Nanolith. Mem. **13**, 041411 (2014).
25. H. X. Guo, H. Itoh, C. M. Wang, H. Zhang, and D. Fujita, "Focal depth measurement of scanning helium ion microscope," Appl. Phys. Lett. **105**(2), 023105 (2014).
26. Y. S. Ku, "Spectral reflectometry for metrology of three-dimensional through-silicon vias," J. Micro-Nanolith. Mem. **13**, 011209 (2014).
27. R. M. Silver, B. M. Barnes, N. F. Zhang, H. Zhou, A. Vladar, J. Villarrubia, J. Kline, D. Sunday, and A. Vaid, "Optimizing hybrid metrology through a consistent multi-tool parameter set and uncertainty model," Proc. SPIE **9050**, 905004 (2014).
28. A. Vaid, C. Osorio, J. Tsai, C. Bozdog, M. Sendelbach, E. Grubner, R. Koret, and S. Wolfling, "Hybrid metrology universal engine: co-optimization," Proc. SPIE **9050**, 905009 (2014).
29. A. E. Vladar, J. S. Villarrubia, J. Chawla, B. Ming, J. R. Kline, S. List, and M. T. Postek, "10 nm three-dimensional CD-SEM metrology," Proc. SPIE **9050**, 90500A (2014).
30. R. Attota, R. M. Silver, M. R. Bishop, and R. G. Dixson, "Optical critical dimension measurement and illumination analysis using the through-focus focus metric - art. no. 61520K," P. Soc. Photo-Opt. Ins. **6152**, K1520 (2006).
31. R. Attota, R. M. Silver, M. Stocker, E. Marx, J. Jun, M. Davidson, and R. Larrabee, "A new method to enhance overlay tool performance," Metrology, Inspection, and Process Control for Microlithography Xvii, Pts 1 and 2 **5038**, 428–436 (2003).
32. R. Attota, R. Silver, and B. M. Barnes, "Optical through-focus technique that differentiates small changes in line width, line height and sidewall angle for CD, overlay, and defect metrology applications," Metrology, Inspection, and Process Control for Microlithography Xxii, Pts 1 and 2 **6922**(2008).
33. S. I. Association, *The International Technology Roadmap for Semiconductors (ITRS)* (Semiconductor Industry Association, 2011).
34. R. Attota, T. A. Germer, and R. M. Silver, "Through-focus scanning-optical-microscope imaging method for nanoscale dimensional analysis," Opt. Lett. **33**(17), 1990–1992 (2008).
35. R. Attota, R. Silver, and R. Dixson, "Linewidth measurement technique using through-focus optical images," Appl. Opt. **47**(4), 495–503 (2008).
36. R. Attota, D. G. Seiler, A. C. Diebold, R. McDonald, A. Chabli, and E. M. Secula, "TSOM method for nanoelectronics dimensional metrology," AIP Conf. Proc. **1395**, 57–63 (2011).
37. R. Attota, R. G. Dixson, J. A. Kramar, J. E. Potzick, A. E. Vladar, B. Bunday, E. Novak, and A. Rudack, "TSOM method for semiconductor metrology," Proc. SPIE **7971**, 79710T (2011).
38. R. Attota and R. Silver, "Nanometrology using a through-focus scanning optical microscopy method," Meas. Sci. Technol. **22**(2), 024002 (2011).
39. A. Arceo, B. Bunday, V. Vartanian, and R. Attota, "Patterned defect & CD metrology by TSOM beyond the 22 nm node," Proc. SPIE **8324**, 83240E (2012).
40. A. Arceo, B. Bunday, and R. Attota, "Use of TSOM for sub-11 nm node pattern defect detection and HAR features," Proc. SPIE **8681**, 86812G (2013).
41. R. Attota and V. Jindal, "Inspecting mask defects with through-focus scanning optical microscopy," SPIE Newsroom, 4964 (2013).
42. R. Attota, B. Bunday, and V. Vartanian, "Critical dimension metrology by through-focus scanning optical microscopy beyond the 22 nm node," Appl. Phys. Lett. **102**(22), 222107 (2013).

43. M. Ryabko, S. Koptyev, A. Shchekin, and A. Medvedev, "Improved critical dimension inspection for the semiconductor industry," SPIE Newsroom, 5515 (2014).
44. M. Ryabko, S. Koptyaev, A. Shcherbakov, A. Lantsov, and S. Y. Oh, "Motion-free all optical inspection system for nanoscale topology control," Opt. Express **22**(12), 14958–14963 (2014).
45. M. Ryabko, A. Shchekin, S. Koptyaev, A. Lantsov, A. Medvedev, A. Shcherbakov, and S. Y. Oh, "Through-focus scanning optical microscopy (TSOM) considering optical aberrations: practical implementation," Opt. Express **23**(25), 32215–32221 (2015).
46. S. E. M. I. document, *Guide for metrology techniques to be used in measurement of geometrical parameters of through- silicon vias (TSVs) in 3DS-IC structures* (SEMI, 2013).
47. V. Vartanian, R. Attota, H. Park, G. Orji, and R. A. Allen, "TSV reveal height and dimension metrology by the TSOM method," Proc. SPIE **8681**, 86812F (2013).
48. R. Attota and R. G. Dixson, "Resolving three-dimensional shape of sub-50 nm wide lines with nanometer-scale sensitivity using conventional optical microscopes," Appl. Phys. Lett. **105**(4), 043101 (2014).
49. B. Bunday, T. A. Germer, V. Vartanian, A. Cordes, A. Cepler, and C. Settens, "Gaps analysis for CD metrology beyond the 22 nm node," Metrology, Inspection, and Process Control for Microlithography XXVII **8681**, 86813B (2013).
50. S. N. Koptyaev, M. V. Ryabko, and M. N. Rychagov, "Optical measurement system and method for measuring critical dimension of nanostructure " US patent (2013).
51. S. N. Koptyaev, M. V. Ryabko, A. V. Hcherbakov, and A. D. Lantsov, "Optical measuring system and method of measuring critical size," US patent (2014).
52. R. Attota, "Noise analysis for through-focus scanning optical microscopy," Opt. Lett. **41**(4), 745–748 (2016).
53. J. M. Gineste, P. Macko, E. A. Patterson, and M. P. Whelan, "Three-dimensional automated nanoparticle tracking using Mie scattering in an optical microscope," J. Microsc. **243**(2), 172–178 (2011).

---

1. Introduction

In the areas of the semiconductor industry and nanotechnology, three-dimensional (3-D) shape evaluation of components is becoming increasingly critical [1, 2], especially for process control. Several metrology tools are currently available [1–32], including for 3-D shape evaluation, with each tool having certain advantages and disadvantages. Low-cost and high-throughput are two of the many requirements for industrial applications, in addition to satisfactory measurement sensitivity and resolution as per the International Technology Roadmap for Semiconductors (ITRS) [33]. Popular industrial metrology tools currently used to evaluate 3-D shape in the semiconductor industry are electron based tools (e.g. scanning electron microscopy (SEM)), probe based tools (e.g. atomic force microscope (AFM)), and optics-based tools (e.g. scatterometry). The National Institute of Standards and Technology (NIST) pioneered the x-ray based tool referred to as critical dimension small angle x-ray scattering (CD-SAXS) [4, 22] that has attracted much industrial attention. A hybrid metrology method initially pioneered at NIST further improved the measurement resolution [27, 28].

Through-focus scanning optical microscopy (TSOM) is another optical metrology method developed at the NIST that demonstrated 3-D shape analysis capability with sub-nanometer measurement resolution using low-cost, conventional optical microscopes [34–45]. TSOM is ideally suitable as a 3-D shape process monitoring tool for high-volume manufacturing (HVM). TSOM can analyze the 3-D shape of target sizes ranging from sub-10 nm to over 100 µm; including isolated as well as repeated structures. For this reason, it needs only a fraction of the target size compared to a scatterometry target [42], and hence has the potential for in-die metrology. TSOM can analyze truly 3-D, deep structures such as through silicon vias and high aspect ratio trenches or vias [46, 47]. In addition, it can reduce the effects of optical cross-correlation, making it less ambiguous to identify the dimensional variations that are leading to the observed optical signal [37, 38]. Three-dimensional shape analysis of isolated sub-50 nm wide lines with sub-nanometer measurement resolution was experimentally demonstrated using the visible illumination wavelength of 546 nm [48]. Measurement sensitivity of less than 0.1 nm was revealed for sub-25 nm wide lines (critical dimensions (CDs)) again using 546 nm wavelength [42]. TSOM is increasingly recognized as a viable nanometrology method, as evidenced by being listed in several technology road maps and guides [33, 46, 49], patent applications [50, 51], and science news reports [41, 43].

A TSOM image is a vertical cross-section constructed from the four-dimensional (4-D) optical data [48] acquired using a conventional optical microscope as a target is scanned along the focus direction [34, 37, 38]. In a TSOM image the X (horizontal), Y (vertical), and

#262754 Received 8 Apr 2016; revised 30 May 2016; accepted 30 May 2016; published 23 Jun 2016

color scale axes represent the spatial position across the target (e.g. along a cross-section line), the focus position, and the optical intensity, respectively. A differential TSOM (D-TSOM) image produced by subtracting two TSOM images (usually obtained using two targets) highlights the 3-D shape difference in the targets down to a sub-nanometer scale [42, 48]. In addition, the D-TSOM image patterns are distinct for different types of parameter changes but qualitatively similar for different magnitude changes in the same parameter [34, 37, 38]. The optical intensity contained in a D-TSOM (or a TSOM) is quantified using the optical intensity range (OIR) [42, 48], defined as the absolute difference between the maximum and the minimum of the normalized optical intensity multiplied by 100. The practical steps to obtain a D-TSOM image are shown as a flow chart in Fig. 1.

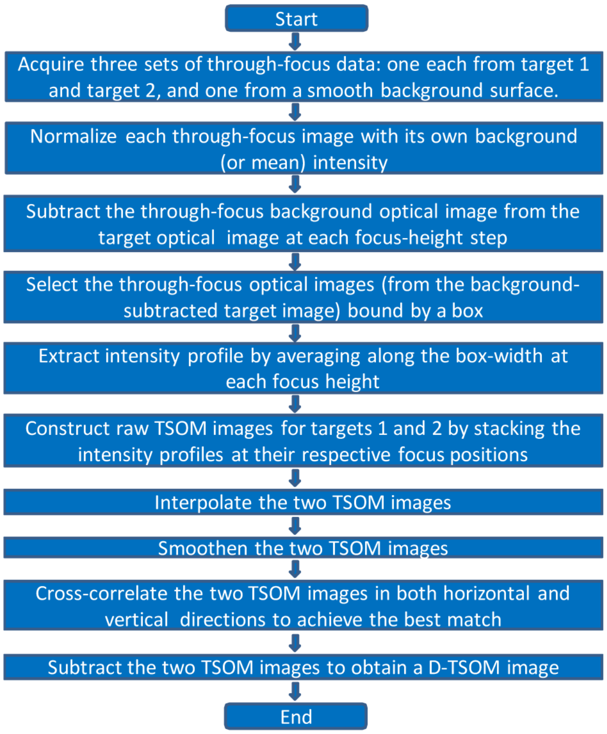
Start
Acquire three sets of through-focus data: one each from target 1 and target 2, and one from a smooth background surface.
Normalize each through-focus image with its own background (or mean) intensity
Subtract the through-focus background optical image from the target optical image at each focus-height step
Select the through-focus optical images (from the background-subtracted target image) bound by a box
Extract intensity profile by averaging along the box-width at each focus height
Construct raw TSOM images for targets 1 and 2 by stacking the intensity profiles at their respective focus positions
Interpolate the two TSOM images
Smoothen the two TSOM images
Cross-correlate the two TSOM images in both horizontal and vertical directions to achieve the best match
Subtract the two TSOM images to obtain a D-TSOM image
End

Fig. 1. Flow chart showing the steps taken to construct TSOM and D-TSOM images.

Optimization of optical system parameters to reduce the total imaging system noise is an important initial step, which we discussed in a previous publication [52]. We showed that the best balance between signal-to-noise performance and acquisition time could be achieved by judicious spatial averaging. Correct background-signal subtraction of the imaging-system inhomogeneities is also critical, as well as the careful alignment of the constituent images used in the analysis. After optimizing the optical system noise, the next logical step is to optimize the experimental parameters (or conditions) to enhance the sensitivity to the dimensional difference. Here we optimize the basic parameters such as illumination numerical aperture (NA), collection NA, focus step height, camera pixels, illumination polarization, and illumination wavelength. In the end, we also briefly discuss methods to enhance the throughput of TSOM.

2. Experiments

We used the following optimization procedure. Two isolated Si lines (nominally 31 nm and 38 nm linewidths and 70 nm height) on a Si substrate were selected as the targets. The fabrication of the targets is similar to that reported earlier [42, 52]. D-TSOM images from

#262754 Received 8 Apr 2016; revised 30 May 2016; accepted 30 May 2016; published 23 Jun 2016
(C) 2016 OSA

these two targets were obtained under the different parametric conditions. The varying magnitudes of the OIR from the D-TSOM image represent the sensitivity of TSOM (for the given fixed linewidth difference). The aim here is to maximize the sensitivity (i.e. OIR) and increase the throughput (without or minimally sacrificing the sensitivity) by optimizing the controllable experimental parameters such as illumination NA (INA), collection NA (CNA), focus step height, camera pixels, illumination polarization, and illumination wavelength. The absolute difference in the magnitude of the selected linewidths is irrelevant as the linewidth difference remains the same under all the experimental conditions. Only the OIRs (of the D-TSOM images) change based on the parametric conditions. Under these conditions, the TSOM sensitivity is proportional to the magnitude of the OIR of a given D-TSOM image.

The TSOM data were acquired using a bright-field, reflection mode optical microscope. Two band-pass filtered LED sources were used to obtain 520 nm and 405 nm illumination wavelengths (λ). The filter used allows a full-width half-max band pass of approximately 10 nm. Other microscopic conditions are similar to that reported in [52]. As depicted in Fig. 1, each analysis requires three through-focus data sets under the same experimental conditions: two data sets using the two selected isolated lines, and one data set using a smooth, clean surface from the test samples. The third data set (from the smooth Si surface) is required to eliminate the optical system (or background) noise from the two target data sets [52]. The parameters used in this study are as close as possible to the noise-optimized base parameters suggested before [52]: smoothing filter span = 400 nm, box width = 0.5 µm, camera pixel scale = 65 nm/pixel, interpolated pixel scale = 20 nm/pixel, optical image signal strength = 100 A.U., focus step size = 300 nm. Of course, when the effect of a parameter is studied, only that parameter would be varied keeping all the other parameters constant. A detailed description of these parameters can be found in [52]. The TSOM analysis was done using the software developed at NIST. Each result given below is an average of 5 repeats. The standard deviations (as a percentage) of the OIR values for the TSOM images varied from about 0.5% to 1.5%.; while for the D-TSOM images they varied from about 2% to 6%. There is approximately 7% standard deviation in the reported INA measurements. CNA values are from the manufacturer of the objectives.

3. Results and discussion

In a reflection type of microscope (as is the one used in the current study), both illumination of the target and collection of the scattered light from the target occurs through the same objective. The illumination cone of light is illustrated in Fig. 2(a). The light scatters in many directions. However, only the scattered light that is within the collection cone (constrained by CNA) of the objective (Fig. 2(b)) enters the microscope and forms the image. CNA is usually fixed for a given objective. However, INA can be easily varied by adjusting the condenser aperture diaphragm. Here, we first discuss the effect of varying INA (Figs. 2(c) and 2(d)) and CNA (Figs. 2(e) and 2(f)) on the TSOM sensitivity.

One of the parameters that has a strong influence on sensitivity when using the TSOM method of analysis is INA. The effect of INA on the OIR of the TSOM and the D-TSOM images is shown in Fig. 3 (by keeping the other parameters constant). Starting from Fig. 3 onwards, all the TSOM images shown will be for the linewidth of 31 nm. The OIR of the TSOM, as well as the D-TSOM images, increases with decreasing INA, showing that the TSOM sensitivity increases with decreasing INA. In addition, the optical information captured by the TSOM image also increases with decreasing INA as can be observed by the increased degree of the color pattern (i.e. optical information). In fact, a dramatic change in the TSOM image color pattern can be observed for the INAs changing from 0.85 to 0.15. In other words, the TSOM image contains richer optical information regarding the target at a lower INA. The optical signal (i.e. intensity pattern) in the TSOM method extends both horizontally (larger signal) and vertically (through a larger focus range) with decreasing INA. This phenomenon can be explained using optical coherence. Decreased INA increases optical coherence and results in an interference or diffraction optical signal that extends both horizontally and vertically in a TSOM image. This condition is beneficial to TSOM type of

#262754 Received 8 Apr 2016; revised 30 May 2016; accepted 30 May 2016; published 23 Jun 2016
(C) 2016 OSA

analysis. This desirable property is exactly opposite to the conventional microscopy design, where much emphasis is given to reducing the optical coherence so that the image appears sharp as in Figs. 3(c) and 3(c').

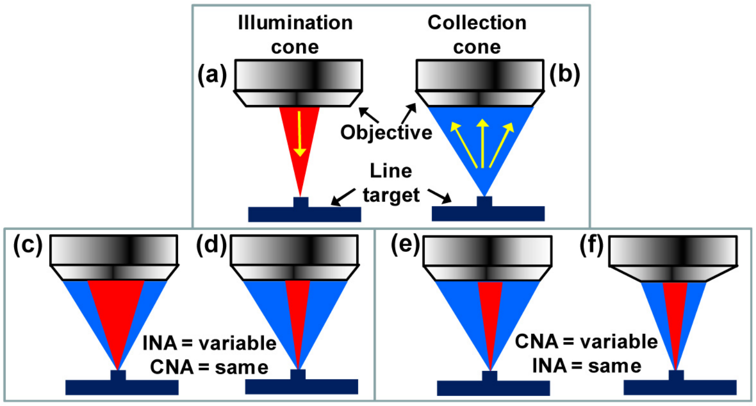

Fig. 2. Schematic of an objective showing (a) illumination (red), and (b) collection (blue) cones. Collection cone (CNA) depends on the NA of the objective and is fixed. Illumination cone (or INA) can be varied by changing the aperture diaphragm. Schematic of an objective showing (c) large, and (d) small INAs for a fixed CNA; and (e) large, and (f) small CNAs for a fixed INA.

Here we demonstrate the effect of NA of the objective (CNA) by using two objectives with two different CNAs (0.55 and 0.85). The condenser aperture diaphragm was adjusted for the selected two objectives such that their INAs are the same, and hence, the effect of CNA can be isolated. The effect of CNA on the TSOM sensitivity is shown in Fig. 4. In this case, the larger CNA shows a higher sensitivity (OIR increases from 7.3 to 9.6). At a given fixed INA, the scattered light is nearly the same irrespective of the CNA as the targets are the same. However, the amount of scattered light entering the objective (to form the image) increases with increasing CNA. In other words, more optical information from the targets is collected by the objective with increasing CNA, thus enhancing the sensitivity.

In general, when the OIR of a TSOM image increases as a function of the change in any given parameter, then usually the corresponding D-TSOM signal strength also increases, and vice-versa. However, under the current experimental conditions, the wavelength of the illumination has the opposing effect on the OIRs of the TSOM and the D-TSOM images. When the λ was reduced from 520 nm to 405 nm, OIRs of the TSOM images increased [Figs. 5(a) and 5(b)], but OIR of the D-TSOM images decreased [Figs. 5(a') and 5(b')]. A similar reduction in sensitivity to line width with decreased λ was reported in a previous publication where TSOM images were obtained using optical simulations [42], supporting the experimental observations made here. However, in the case of defect analysis, in nearly every case the lower λ increases defect detection (i.e. increases sensitivity) [39]. The defect and linewidth examples presented here highlight that a generalized statement for TSOM sensitivity cannot be made with respect to λ, perhaps due to the dependence of optical properties and penetration depth with λ.

#262754 Received 8 Apr 2016; revised 30 May 2016; accepted 30 May 2016; published 23 Jun 2016

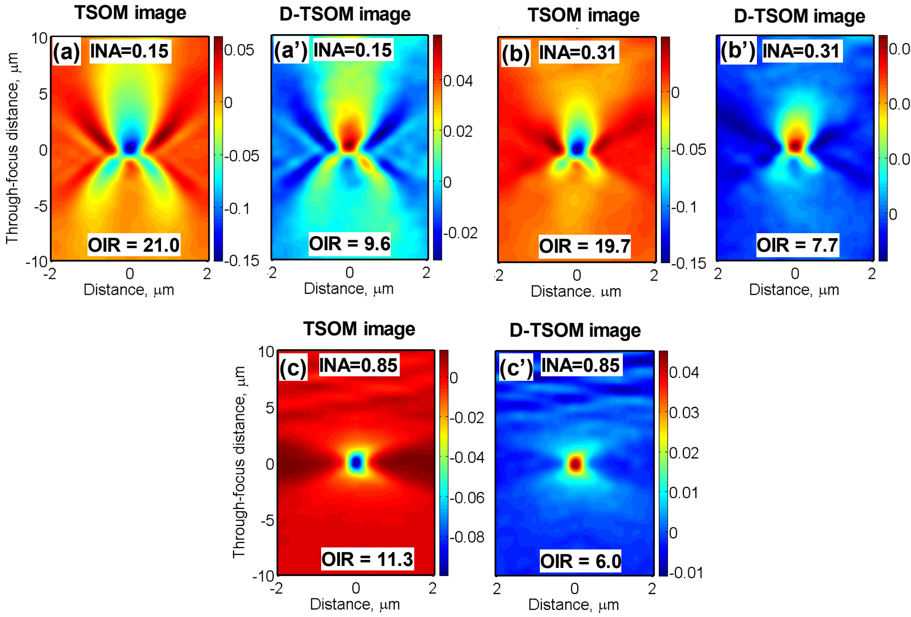

Fig. 3. Figure showing the effect of the illumination NA (INA) on TSOM sensitivity. (a), (b) and (c) TSOM images for INAs of 0.15, 0.31 and 0.85, respectively. (a'), (b') and (c') D-TSOM images for INAs of 0.15, 0.31 and 0.85, respectively. CNA = 0.85, Focus step size = 300 nm, Camera pixel scale = 32 nm/pixel, Interpolated pixel scale = 16 nm/pixel, λ = 520 nm, 90° polarized light.

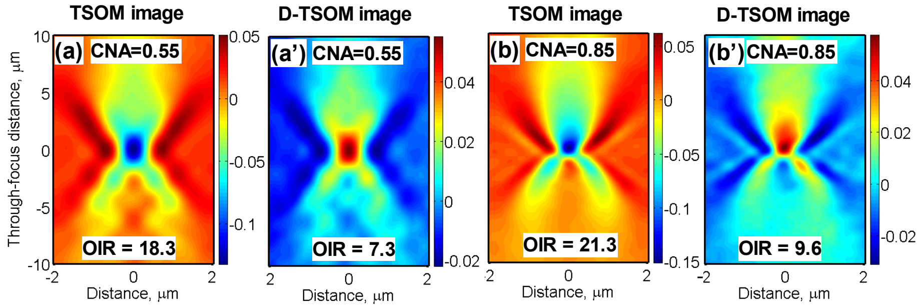

Fig. 4. Figure showing the effect of the collection NA (CNA) on TSOM sensitivity. (a) and (b) TSOM images for CNAs of 0.55 and 0.85, respectively. (a') and (b') D-TSOM images for CNAs of 0.55 and 0.85, respectively. INA = 0.15, Focus step size = 300 nm, Camera pixel scale = 32 nm/pixel, Interpolated pixel scale = 16 nm/pixel, λ = 520 nm, 90° polarized light.

Since TSOM is an optical method, a small change in the 3D shape of a target produces a change in the optical signal that spreads over a large lateral distance [48]. For example, under the current experimental conditions, a nominally 7 nm difference in the linewidth produced a lateral change in the D-TSOM optical signal spreading over a micrometer. Therefore, a relatively large camera pixel scale (or low camera pixel count) can still adequately detect these large-scale lateral changes in the signal. Camera pixel scales such as 16 nm/pixel [5.8 mega pixel (MP), Fig. 6(a)], 65 nm/pixel [0.36 MP, Fig. 5(a)] and 161 nm/pixel [0.056 MP, Fig. 6(b)] produced a similar sensitivity to the fixed linewidth difference showing that the dimensional sensitivity as detected by TSOM is robust to camera pixel resolution (or camera pixel scale). However, noise increases with increased pixel scale [52], which could be the reason for the small difference in the TSOM sensitivity observed in Fig. 6. This shows that a relatively small number of pixels (or a low MP camera) could successfully be used with the TSOM method of analysis.

#262754 Received 8 Apr 2016; revised 30 May 2016; accepted 30 May 2016; published 23 Jun 2016
(C) 2016 OSA

When we compare Figs. 4(a) and 4(a’) with Figs. 5(a) and 5(a’) we can realize that polarization of the illumination has a significant effect on the TSOM sensitivity. In the current case, the 90° polarized light (electric field parallel to the line) has higher sensitivity compared to the un-polarized light. However, this may not be the case under all the conditions and hence the polarization sensitivity needs to be optimized for a given condition.

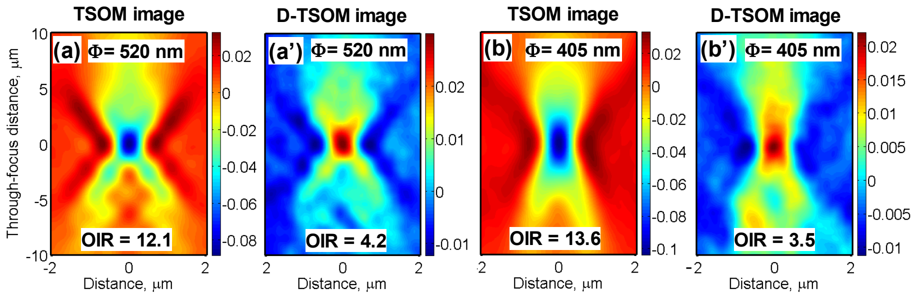

Fig. 5. Figure showing the effect of the illumination wavelength (λ) on TSOM sensitivity. (a) and (b) Processed TSOM images for λ = 520 nm, and λ = 405 nm, respectively. (a’) and (b’) D-TSOM images for λ = 520 nm, and λ = 405 nm, respectively. INA = 0.15, CNA = 0.55, Focus step size = 300 nm, Camera pixel scale = 65 nm/pixel, Interpolated pixel scale = 20 nm/pixel, un-polarized light.

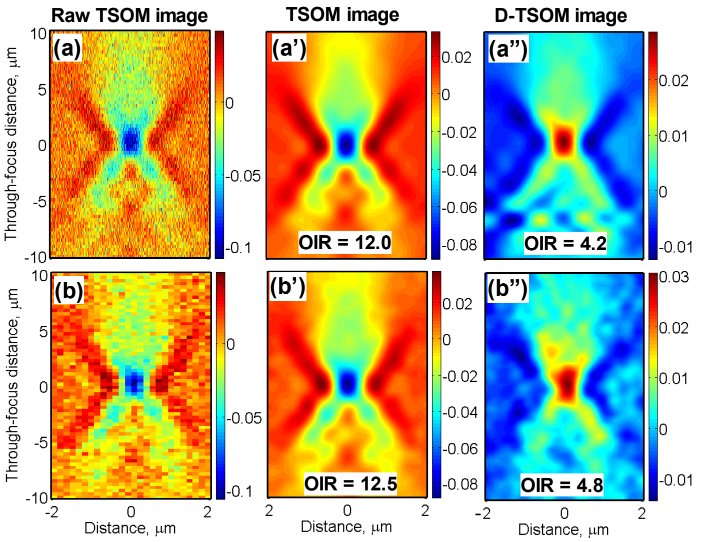

Fig. 6. Figure showing the effect of the camera pixel scale on TSOM sensitivity. (a) and (b) Raw TSOM images for camera pixel scales of 16 nm/pixel (5.8 MP), and 161 nm/pixel (0.056 MP), respectively. (a’) and (b’) Processed TSOM images for camera pixel scales of 16 nm/pixel, and 161 nm/pixel, respectively. (a”) and (b”) D-TSOM images for camera pixel scales of 16 nm/pixel, and 161 nm/pixel, respectively. INA = 0.15, CNA = 0.55, Focus step size = 300 nm, Interpolated pixel scale ~20 nm/pixel, λ = 520 nm, un-polarized light.

Figure 7 shows the effect of focus step size on the TSOM sensitivity. For the three step sizes used, a similar sensitivity can be observed. The similar explanation given to the pixel scale can be provided for the focus step also, as the optical signal in the D-TSOM image extends through a large focus distance making it possible to use large step sizes, adequately.

In Fig. 6, pixel scale was increased up to 161 nm/pixel by keeping a fixed focus step size of 300 nm, while in Fig. 7, focus step size was increased up to 2000 nm by keeping a fixed camera pixel scale of 65 nm/pixel. Under these two kinds of varying conditions, the TSOM sensitivity remains approximately the same. Here we increase both the focus step size and the camera pixel scale simultaneously to determine the maximum values where the TSOM starts to break down. It was found that up to a focus step size of 1500 nm and a pixel scale of 161 nm, TSOM continues to show sensitivity to the given linewidth difference with nearly similar appearing TSOM and D-TSOM image patterns (Fig. 8); however, the sensitivity is reduced. Under these extreme conditions, the raw TSOM image has a total pixel count of 375, indicating that TSOM continues to detect the nanometer scale difference with extremely low image pixel count (ideally suitable for high-throughput applications).

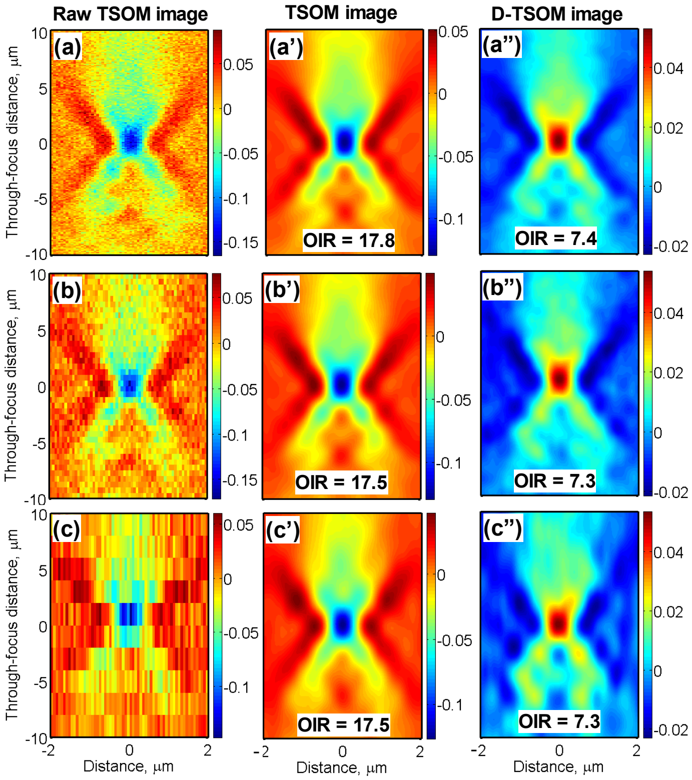

Fig. 7. Figure showing the effect of the focus step size on TSOM sensitivity. (a), (b) and (c) Raw TSOM images for focus steps of 100 nm (250 images), 500 nm (50 images) and 2000 nm (12 images), respectively. (a'), (b') and (c') Processed TSOM images for focus steps of 100 nm, 500 nm and 2000 nm, respectively (linewidth = 31 nm). (a"), (b") and (c") D-TSOM images for focus steps of 100 nm, 500 nm and 2000 nm, respectively. INA = 0.15, CNA = 0.55, Camera pixel scale = 65 nm/pixel, Interpolated pixel scale = 20 nm/pixel, λ = 520 nm, 90° polarized light.

TSOM inherently requires several through-focus images. Reducing the number of through-focus images needed can effectively reduce the acquisition time and hence increase throughput. Here we evaluate the minimum number of TSOM images required to obtain a sensitivity similar to under the standard conditions used in the above paragraphs (with approximately an OIR of 7.3 for the D-TSOM image). It was found that as low as six through-focus images at a focus step size of 2000 nm, but with 65 nm/pixel scale were sufficient to get an OIR of 7.3 for the D-TSOM image (Fig. 9). By optimizing the camera pixel size, focus step size, and number of focus steps required, the throughput of TSOM can be enhanced. An acquisition time of 200 ms for 100 focus steps has already been demonstrated in the laboratory [53]. If the number of focus steps required is less than 100 (say, for example, 20), then the TSOM acquisition time can be significantly less than 200 ms, enabling high-throughput TSOM measurements.

Received 8 Apr 2016; revised 30 May 2016; accepted 30 May 2016; published 23 Jun 2016
(C) 2016 OSA

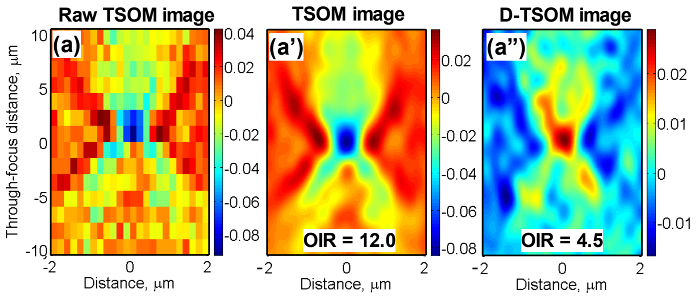

Fig. 8. Test to determine the minimum number of pixels in a TSOM image needed to get sufficient sensitivity. (a) Raw TSOM image constructed with 375 pixels. (b) Processed TSOM image. (d) D-TSOM image. INA = 0.15, CNA = 0.55, Focus step = 1500 nm, Camera pixel scale = 161 nm/pixel, Interpolated pixel scale = 20 nm/pixel, λ = 520 nm, un-polarized light.

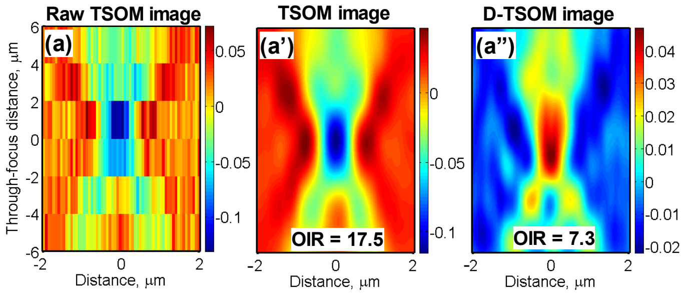

Fig. 9. Test to determine the minimum number of focus steps needed for the TSOM analysis. (a) Raw TSOM image with 6 focus steps. (b) Processed TSOM image. (d) D-TSOM image. INA = 0.15, CNA = 0.55, Focus step = 2000 nm, Camera pixel scale = 65 nm/pixel, Interpolated pixel scale = 20 nm/pixel, λ = 520 nm, 90° polarized light.

In summary, the current study shows that optimizing parametric conditions is important for obtaining the highest sensitivity using TSOM. Low illumination NA and high collection NA enhance TSOM sensitivity as do appropriately chosen illumination polarization and wavelength. Depending on the application, large focus step sizes and large camera pixel scales (i.e. low MP cameras) can be adequately used with acceptable sensitivity. In other words, TSOM requires less stringent conditions than the other tools to obtain nanometer scale 3D shape sensitivity.

Disclaimer

Any mention of commercial products or entities in this paper is for informational purposes only; it does not imply recommendation or endorsement by NIST.

Acknowledgments

The authors would like to thank Richard Kasica of CNST, for providing the sample; and John Kramar for the useful discussions.